Journal

Origin of Different Growth Modes for Epitaxial Manganite Films

Rongsheng Cai,[‡] Yiqian Wang,[‡,†] Xuehua Liu,[‡] Weiwei Gao,[§] Yunzhong Chen,[§]
Jirong Sun,[§] and Yanguo Wang[¶]

[‡]The Cultivation Base for State Key Laboratory, Qingdao University, No. 308 Ningxia Road, Qingdao 266071, China

[§]State Key Laboratory of Magnetism and Beijing National Laboratory for Condensed Matter Physics, Institute of Physics,
Chinese Academy of Sciences, Beijing 100080, China

[¶]Laboratory of Advanced Materials and Electron Microscopy, Institute of Physics, Chinese Academy of Sciences,
Beijing 100080, China

The microstructures of the $Bi_{0.4}Ca_{0.6}MnO_3$ (BCMO) and $La_{0.67}Ca_{0.33}MnO_3$ (LCMO) epitaxial films are investigated by transmission electron microscopy in detail. BCMO epitaxial films (~ 10 and ~ 40 nm) exhibit an island growth mode whereas the LCMO films (~ 6 and ~ 30 nm) follow a layer by layer growth mode. Combined with the critical thickness models for the expected onset of the misfit dislocations in epitaxial films, an atomic collapse model is introduced to explain their mechanism of formation in manganite films. At the beginning of deposition, the strain caused by the lattice mismatch between the epitaxial film and substrate can be accommodated by elastic deformation. With the increase of film thickness, the strain becomes larger and larger. When the film thickness reaches the critical thickness, the strain can only be relaxed by the formation of misfit dislocations. Meanwhile, the atomic configuration of the epitaxial film will reorganize and some atoms begin to collapse, thus an island morphology will be formed. Once the collapse morphology is formed, maintenance of this wave-like morphology depends on atomic diffusion length of the deposited atoms. If the diffusion length of the deposited atoms is long, the island morphology will not be maintained. If the diffusion length of the deposited atoms is short, the island morphology will keep until the epitaxial film is thick enough. The results could shed light on the growth modes for other perovskite epitaxial films.

I. Introduction

RECENTLY, perovskite manganites of the formula $R_{1-x}A_xMnO_3$ (R being a trivalent rare earth and A being a divalent alkaline-earth ion) have received considerable attention[1–5] due to the colossal magnetoresistance effect. The perovskite manganite films have great potential for a wide range of applications in the field of high-speed magnetic storage device and photoelectronic device.[6–8] The comprehensive understanding of the growth mechanism for the epitaxial perovskite films can help us improve their preparation process.

Three different growth modes for metal and semiconductor epitaxial films have been reported: a layer by layer growth mode,[9–11] an island growth mode,[12–15] and a layer by layer plus an island growth mode.[16–20] Frank-van der Merwe,[21] Volmer-Weber,[22] and Stranski-Krastanow[23] have proposed different models, FvdM, VW, and SK models, to explain the three types of growth modes, respectively. Generally, the growth mode of thin films is greatly influenced by interfacial energy during the epitaxial growth process. Frank-van der Merwe found that if the lattice mismatch between film and substrate is relatively small, the film can grow two dimensionally under certain growth conditions. In this growth mode, if the growing layer is thinner than a critical thickness, the strain generated by lattice mismatch is elastically accommodated within the growth layer, and a coherent interface will eventually be produced.[24] If the film thickness exceeds the critical thickness, the introduction of mismatch dislocations is energetically favored and the dislocations will relieve some strain to form a semicoherent interface. This mechanism has been discussed by Matthews and others[25,26] in detail. Theoretical equilibrium calculations of the critical thickness predict when dislocations will form but do not explore the correlation between the growth mode and the occurrence of misfit dislocations.

For manganite epitaxial films, Lebedev *et al.*[27] have investigated the growth process of $La_{0.7}Sr_{0.3}MnO_3$ film grown on $LaAlO_3$ substrate. They found that the epitaxial film initially grows layer by layer, and then the epitaxial islands coalesce together, which belongs to an SK growth mode. However, the detailed information of the coalescence process was not given. As for the relationship between the mismatch dislocation and the growth morphology, quite few investigations can be found using transmission electron microscopy (TEM). Some researchers replaced the A ion with different divalent ions and explored the changes in physical properties[28,29] whereas others investigated the influence of the oxygen pressure and deposition temperature on the physical properties.[30] Frey *et al.*[31] demonstrated that the use of atomic oxygen could promote the growth of large area one-unit-cell smooth epitaxial cuprate films. Due to the difficulties in preparing cross-sectional TEM specimens for the epitaxial films thinner than 10 nm, no direct TEM experimental results have been presented to show the influence of the lattice mismatch on the growth modes up to now. So, a detailed investigation on the microstructure of the epitaxial manganite films is highly desired as it could provide significant insights into understanding the growth mechanism for these epitaxial films.

In this study, we report on the microstructural investigation of the $Bi_{0.4}Ca_{0.6}MnO_3$ (BCMO) and $La_{0.67}Ca_{0.33}MnO_3$ (LCMO) epitaxial thin films using high-resolution transmission electron microscopy (HRTEM). From TEM observations of the morphologies for epitaxial films, it is found that BCMO epitaxial film follows an island growth mode whereas LCMO film exhibits a layer by layer growth mode. The critical thickness for the BCMO epitaxial film is much smaller than that of the LCMO epitaxial film. The atomic collapse

model is employed to explain the reasons for the two different growth modes.

II. Experimental Procedures

Epitaxial BCMO films were prepared on a (110) $SrTiO_3$ (STO) substrate by pulsed laser deposition (PLD) technique from a target with a nominal composition of $Bi_{0.4}Ca_{0.6}MnO_3$ (laser wavelength = 248 nm, repetition rate = 5 Hz, and fluency = 7 J/cm^2). During the deposition, the substrate temperature was kept at ~ 700°C and the oxygen pressure at ~ 60 Pa. The film thickness was controlled by the deposition time. X-ray diffraction (XRD) analysis indicates that all the films are a single phase and epitaxially grown on (110) STO substrates.[32]

LCMO films were prepared on a (001) STO substrate using PLD technique from a target with a nominal composition of $La_{0.67}Ca_{0.33}MnO_3$ (laser wavelength = 248 nm, repetition rate = 5 Hz, and fluency = 7 J/cm^2). During the deposition, the substrate temperature was kept at ~ 720°C and the oxygen pressure at ~ 80 Pa. The film thickness was controlled by the deposition time. XRD analysis indicates that the films are a single phase and epitaxially grown on (001) STO substrates.

Specimens for TEM examinations were prepared in a cross-sectional orientation using conventional techniques of mechanical polishing and ion thinning. The ion milling was performed using a Gatan Model 691 precision ion polishing system (PIPS, Pleasanton, CA). The bright field (BF) imaging, selected-area electron diffraction (SAED) and HRTEM examinations were carried out using a (TEM; JEM 2100F, JEOL, Tokyo, Japan) transmission electron microscope operating at 200 kV.

III. Results and Discussion

Figure 1(a) shows a typical BF TEM image of a cross-sectional BCMO/STO sample with a thickness of ~ 10 nm. The BF image was taken under a two-beam condition with $g = 110$. The interface between the substrate and film is indicated by dashed lines. It can be clearly seen from Fig. 1(a) that the free surface of the epitaxial film is not flat. And the morphology of the film is more like a wave or an island. The height of the highest wave crest is about 12 nm, while the height of lowest wave trough is around 8 nm. The average height and width of the waves are ~ 10 and ~ 40 nm, respectively. So, we conclude that the strained ultrathin (~ 10 nm)

epitaxial film exhibits a 3-D island growth mode. Figure 1(b) is the SAED pattern taken from the epitaxial film region, which corresponds to a $[\bar{1}11]$ zone-axis diffraction pattern of BCMO. From the diffraction pattern, it confirms that the BCMO film is single crystalline and the growth direction of the film is along [110]. Figure 1(c) is a typical $[\bar{1}11]$ zone-axis HRTEM image taken from the interfacial region of BCMO/STO in Fig. 1(a). The interface between the STO substrate and BCMO film is marked by dashed lines. From the enlarged HRTEM image, it is evident that the surface of the film consists of waves or islands. The top of the wave is almost flat, parallel to the interface of the BCMO/STO. The growth direction of the epitaxial film is along [110], and the (110) lattice planes are marked by two parallel lines. The measured interplanar spacing for (110) lattice plane is 2.66 Å, which is a little smaller than the theoretically calculated value of 2.69 Å. The BCMO film has an epitaxial relationship with the STO substrate of $(110)_{BCMO}//(110)_{STO}$ and $[\bar{1}11]_{BCMO}//[\bar{1}11]_{STO}$. Near the interface region of the BCMO and STO, in this image a pure edge dislocation can be seen. To show the extra half atomic plane more clearly, an enlarged HRTEM image of this dislocation is shown in Fig. 1(d), which is taken from the region enclosed by a rectangle in Fig. 1(c). From Fig. 1(d), it is clear that the substrate has an extra half atomic plane. The Burgers vector for this dislocation is determined to be $b = <110>$.

Figures 2(a) and (b) are a typical BF TEM image and SAED pattern, respectively, of a cross-sectional BCMO/STO sample with a film thickness of ~ 40 nm. Similar to Fig. 1, the BF image was taken under a two-beam condition with $g = 110$. It can be seen that the morphology of the film is also similar to a wave with an average height and width of ~ 40 and ~ 100 nm, respectively. Compared with the thinner epitaxial film in Fig. 1(a) (thickness of ~ 10 nm), the surface of the 40-nm-thick epitaxial film is composed of higher and wider waves. The SAED pattern confirms that the thicker BCMO film is also single-crystalline phase and has the growth direction along [110]. Figure 2(c) shows a $[\bar{1}11]$ zone-axis HRTEM image taken from the region enclosed by a rectangle in Fig. 2(a). The interface between STO and BCMO is indicated by dashed lines at the edges. The thicker BCMO film has a similar epitaxial relationship with the STO substrate: $(110)_{BCMO}//(110)_{STO}$ and $[\bar{1}11]_{BCMO}//[\bar{1}11]_{STO}$. To check if dislocations also exist in this film, Fig. 2(c) was carefully analyzed. Pure edge dislocations were found as shown
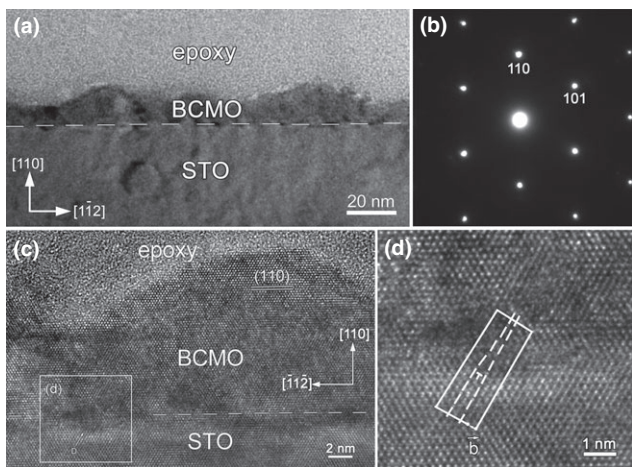

Fig. 1. (a) Cross-sectional BF TEM image of the BCMO/STO epitaxial film with the thickness of about 10 nm; (b) SAED pattern taken from the epitaxial film in (a); (c) Typical HRTEM image taken from the BCMO/STO epitaxial film in (a); (d) Enlarged HRTEM image taken from the interface region enclosed by a rectangle in (c), the misfit dislocation is indicated.
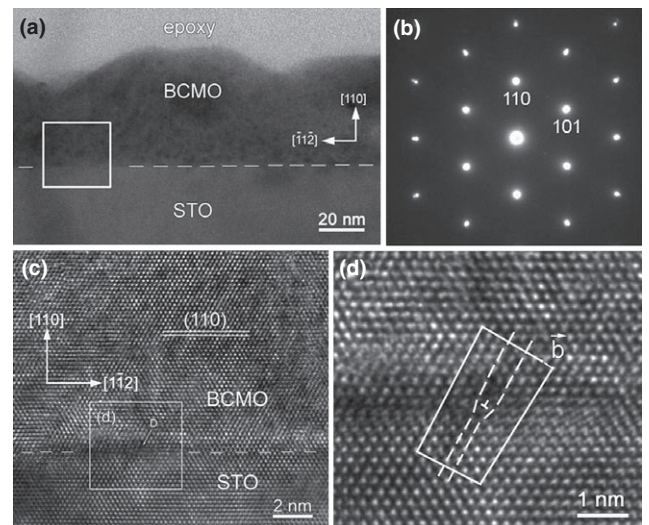

Fig. 2. Cross-section BF TEM image (a) and SAED pattern (b) of the BCMO/STO film with a thickness of about 40 nm; (c) Typical HRTEM image taken from the interface region of BCMO/STO; (d) Enlarged HRTEM image of the region enclosed by a rectangle in (c), the misfit dislocation is marked.
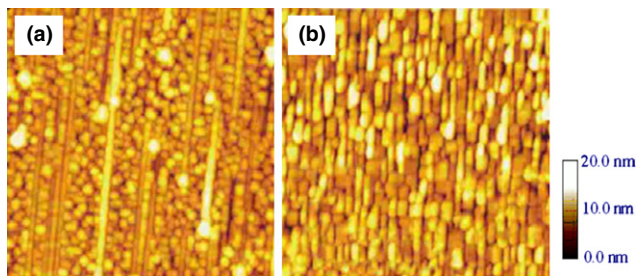
Fig. 3. AFM images of the BCMO epitaxial films with the thickness of 10 nm (a), 40 nm (b).

in the enlarged HRTEM image of Fig. 2 (d). The extra half atomic plane is in the BCMO film like the thinner film of Fig. 1. The Burgers vector is determined to be b = <110>. Figures 3(a) and (b) show a typical 2 μm^2 × 2 μm^2 AFM images for BCMO films with a thickness of 10 and 40 nm, respectively. It can be seen that the surface morphologies of both films exhibit a 3-D island structure. The islands become wider and wider with an increase of the film thickness. This result is consistent with our TEM observations.

From a comparison of the two BCMO films (10 and 40 nm), we can see a tendency for the period of the surface wave morphology to become larger with increasing thickness, as expected for a material relaxing stress. Eventually, the island morphology will disappear. This is consistent with our previous study[15] in which the surface morphology of the BCMO film becomes flat when the film is thicker than 100 nm. So, the growth process for the BCMO films can be deduced as follows. Tiny islands form first on the surface of the STO substrate. With increase of growth time, these islands become larger and larger, eventually coalescing together. At last, the island morphology disappears, and the surface of the BCMO film becomes flat.

Apart from the growth mode, Chen *et al.*[33] investigated the physical properties of BCMO films with different thicknesses. It has been found that for the BCMO films of 10 and 40 nm, the resistivities along [100] and [0$\bar{1}$1] directions are different, and no charge/orbital ordering (CO/OO) transition occurs. While for the 100-nm-thick film, its resistivity is similar to that of bulk material. The resistivities are identical along the [100] and [0$\bar{1}$1] directions, and the CO/OO transition appears. From our observations, it can be found that both 10 and 40 nm films exhibit island morphologies and the stresses along [100] and [0$\bar{1}$1] direction generated by lattice mismatch are different. However, for the film thicker than 100 nm, the surface is atomically flat, and the stress can be completely relieved. So, it can be deduced that lattice stress has a strong effect on the physical properties of the films.

For comparison, the structure of LCMO epitaxial films was also investigated by TEM. Figures 4 (a) and (b) show a typical BF TEM image and SAED pattern, respectively, of a cross-sectional LCMO/STO sample with a film thickness of about 6 nm. The BF image was taken under a two-beam condition with *g* = 002. The interface between LCMO film and STO substrate is indicated by two white arrows. The SAED indicates that the LCMO film is single crystalline and the growth direction for the film is along [001]. In Fig. 4(a), it is obvious that the surface of the film is very flat. Moreover, it can be found that the free surface of the film is parallel to the interface between LCMO and STO. Figure 4(c) is a typical [010] zone-axis HRTEM image taken from the interfacial region of LCMO/STO. The measured film thickness is 6.0 nm. The interesting finding is that the interface between the film and the substrate is coherent. Through TEM observations of many regions around the interface, no evident defects can be found. The film and the substrate have the expected epitaxial relationship of $(001)_{BCMO}$//$(001)_{STO}$ and $[010]_{BCMO}$//$[010]_{STO}$.
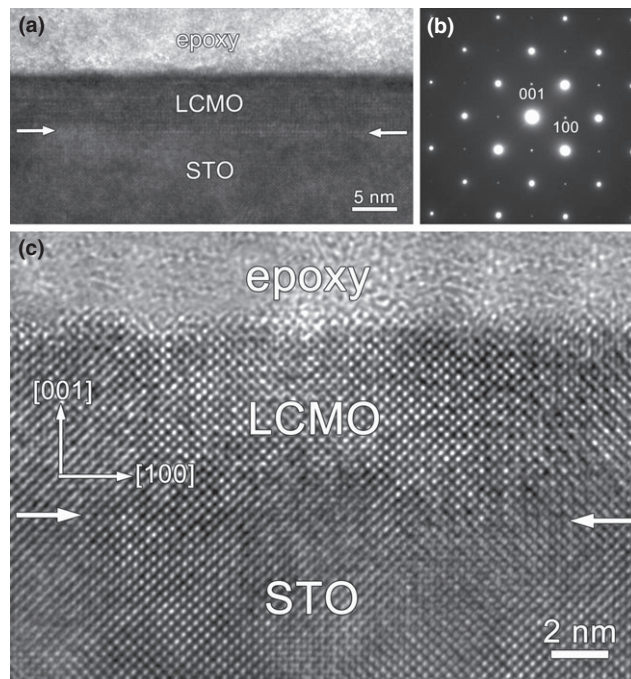

Fig. 4. (a) Cross-section BF TEM image of the LCMO/STO epitaxial film with the thickness of about 6 nm; (b) and (c) SAED pattern and typical HRTEM image taken from the epitaxial film in (a), respectively.
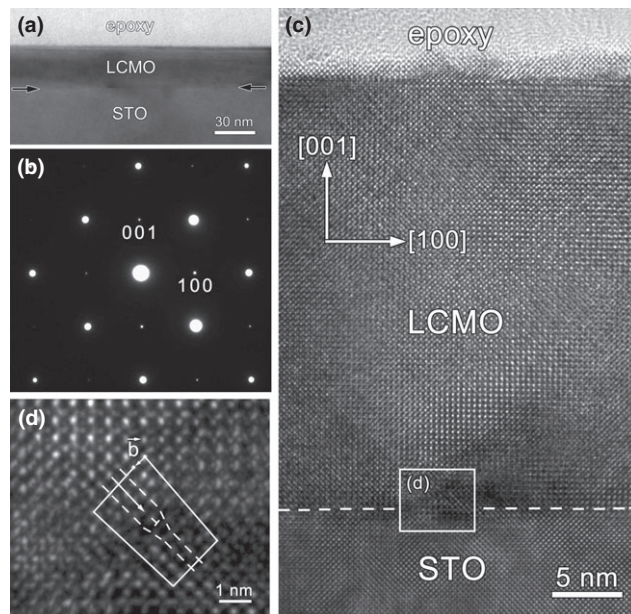

Fig. 5. (a) Cross-section BF TEM image (a) and SAED pattern (b) of the LCMO/STO film with a thickness of ~30 nm; (c) Typical HRTEM image taken from the interface region of LCMO/STO; (d) Enlarged HRTEM image of the region enclosed by a rectangle in (c), the misfit dislocation is depicted.

To clarify the growth process for the LCMO epitaxial film, the LCMO film with a thickness of 30 nm was also examined by TEM. Figures 5 (a) and (b) are a typical BF TEM image and SAED pattern, respectively, of a cross-sectional LCMO/STO sample with a film thickness of 30 nm. The BF image was taken under a two-beam condition with *g* = 002. The interface between LCMO film and STO substrate is marked by two black arrows. The SAED pattern shows that the LCMO film is single crystalline and the growth direction for the film is along [001]. In Fig. 5(a), it is
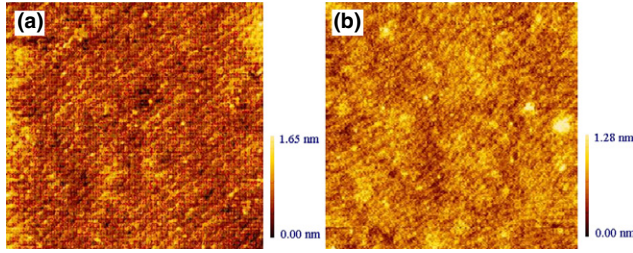
Fig. 6. AFM images of the LCMO epitaxial films with the thickness of 6 nm (a), 30 nm (b).

obvious that the free surface of the film is flat, similar to that in Fig. 4(a). In addition, it can be found that the film surface is parallel to the interface between the LCMO film and STO. Figure 5(c) is a typical [010] zone-axis HRTEM image taken from the interfacial region of LCMO/STO. Pure edge dislocations exist at this interface. An example is shown in the enlarged HRTEM image Fig. 5(d) from the rectangular enclosed area in Fig. 5(c). The LCMO film has an extra half atomic plane as expected. The Burgers vector for the dislocation is determined to be also $b = <110>$. The film and the substrate have a good epitaxial relationship of $(001)_{BCMO}//$ $(001)_{STO}$ and $[010]_{BCMO}//[010]_{STO}$. Figures 6(a) and (b) show the typical 1 $\mu m^2 \times$ 1 μm^2 AFM images for the films with the thickness of 6 and 30 nm, respectively. It can be seen that the free surfaces of both films are smooth. The root mean square surface roughness for both films is about 0.2 nm. The water stripe pattern indicates that the LCMO films have a good epitaxial growth and follow a 2-D growth mode. The AFM result is consistent with our TEM observation. The resistive properties of the LCMO films were also studied.[34] For the thick films (>30 nm), the electronic transport behavior is metallic at low temperatures and semiconducting at high temperatures. In contrast, the thin films (<6 nm) exhibit a monotonic resistivity growth while decreasing temperature in the whole temperature region studied. According to our HRTEM results, in the 6-nm-thick film, the interface is coherent and no mismatch dislocations are observed. While in the 30-nm-thick film, the interface is not coherent and some mismatch dislocations are found. So, it can be deduced that the appearance of the dislocation in the film might be one reason for the different electronic transport behaviors of these two films. Detailed correlation will be discussed elsewhere.

From a comparison of the results for LCMO films with thicknesses of 6 nm and 30 nm, the growth process can be deduced as a layer by layer growth mode. At the beginning, the substrate surface is covered by a thin layer of deposited atoms and no island form. With the increase of the time, the LCMO layer becomes thicker and thicker. During this process, the surface of the film is flat all the time. Eventually, the LCMO epitaxial film forms a smooth and flat surface.

From the above analysis, a very interesting fact is that BCMO and LCMO epitaxial films demonstrate different growth modes. The BCMO films exhibit an island growth mode, whereas the LCMO films follow a layer by layer growth mode. Based on thermodynamic assumptions, Matthews and Blakeslee[26] introduced a model for the onset of misfit dislocations in thin films about 30 yr ago. In our case, BCMO and LCMO epitaxial films grow on the same substrate STO, and the conditions for the epitaxial process are similar. The lattice parameters for the STO substrate and BCMO, and LCMO films are 3.905, 3.790, and 3.868 Å, respectively. Then, the lattice mismatch between a film and substrate can be determined using the formula:

$$f = \left(\frac{a_s - a_f}{a_s}\right) \times 100\%$$

where a_s and a_f refer to the lattice parameters of the substrate and film, respectively. The lattice mismatch (f) is calcu-

lated to be 2.945% and 0.95% for BCMO and LCMO, respectively. The critical thickness, h_c, where an existing dislocation is in mechanical equilibrium can be obtained using the formula:

$$h_c = \frac{\left|\vec{b}\right|}{4\pi f(1 + v)}\left[\ln\left(\frac{h_c}{\left|\vec{b}\right|}\right) + 1\right],^{35}$$

where b is the length of the Burgers vector, f is the lattice mismatch, and v is the Poisson ratio. It should be noted that here the Burgers vector b means the magnitude of its horizontal component, namely, the interplanar spacing of the lattice planes perpendicular to the interface. For BCMO and LCMO in our experiment, it is the interplanar spacing of $(\bar{1}1\bar{2})$ and (100) planes, respectively. The h_c value for BCMO and LCMO films is calculated to be 0.88 and 10.47 nm. For the 6-nm-thick LCMO epitaxial films, the film thickness is smaller than the critical thickness (~ 10.47 nm), and the lattice mismatch is relatively small (~ 0.95%). The strain caused by the lattice mismatch was accommodated by elastic deformation and no dislocations were detected. When the thickness reached 30 nm which is thicker than the critical thickness, the strain cannot be relieved by the elastic deformation, so the dislocations will be formed. For BCMO epitaxial films (~ 10 and ~ 40 nm), they are both thicker than the critical thickness (~ 0.88 nm), and the lattice mismatch is relatively large (~ 2.945%), so the strain generated by the lattice mismatch can only be relaxed by the formation of dislocations.

Based on the critical thickness model, an atomic collapse model is proposed to interpret the growth process for the layer by layer growth mode and the island growth mode. Figure 7 is the schematic diagrams of the atomic collapse model. At the beginning of the epitaxial growth, the film is thinner than the critical thickness. The strain caused by the lattice mismatch can be accommodated by elastic deformation. So, dislocations have not occurred at the interfacial
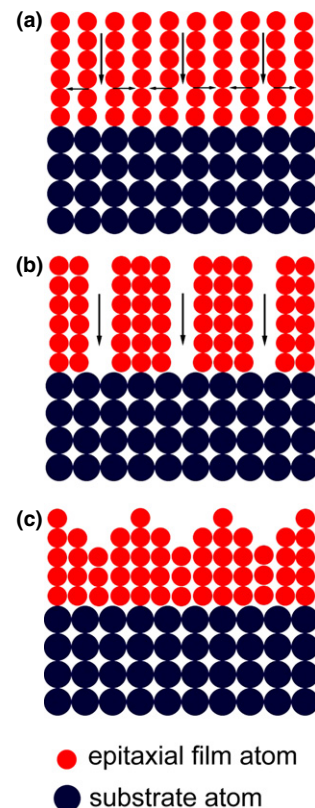

● epitaxial film atom

● substrate atom

Fig. 7. Schematic diagrams for the atomic collapse model.

region, and the interface between the epitaxial film and the substrate is coherent [Fig. 7(a)]. With the increase of time, the film thickness increases and the volume strain energy caused by lattice mismatch becomes larger and larger. When the film thickness reaches the critical thickness, the strain can no longer be accommodated by elastic deformation. Misfit dislocations are formed to relax the strain [Fig. 7(b)]. At this time, the atoms begin to collapse at the central location of the misfit lattices, leading to the formation of collapse morphology [Fig. 7(c)]. The collapse morphology is more like an island. It should be noted that bigger mismatch and the smaller critical thickness will lead to more obvious atomic collapse. Once the dislocations have formed, maintenance of the wave-like morphology depends on the surface atomic diffusion length. If the atomic diffusion length is long, the atoms on the surface will diffuse to the lower energy places, and the collapse morphology will coalesce and disappear eventually. But if the surface atomic diffusion length is short, the atoms on the surface do not have enough energy to diffuse to the lower energy positions, so the collapse morphology will be preserved. Once the film is much thicker than the critical thickness, the growth process is similar to bulk materials. The film surface tends to become flat because of surface free energy minimization. In our experiment, the atomic diffusion length for the BCMO film is not long enough, so once the misfit dislocations formed, the island morphology was maintained. However, the surface atomic diffusion length for the LCMO film is long enough. Once the misfit dislocations formed, the surface atoms diffused to the low energy positions quickly, such that no collapse morphology was observed. Thus, the film followed a layer by layer growth mode.

From the calculation of the critical thickness, it can be deduced that the lattice mismatch *(f)* plays a very important role in the determination of the critical thickness. If *f* is big, the calculated h_c is usually large, and the mismatch dislocations are more easily produced at the interface region. At the same time, the epitaxial film often exhibits an island growth mode. The critical thicknesses for LCMO epitaxial films on (001) NdGaO$_3$ and LaAlO$_3$ substrates were calculated to further demonstrate the importance of the critical thickness in determining the growth mode for epitaxial films. For the LCMO on the NdGaO$_3$ and LaAlO$_3$, the critical thicknesses are 121.02 and 3.86 nm, respectively. The lattice mismatch for LCMO/NdGaO$_3$ is 0.129%, while it is 1.98% for LCMO/LaAlO$_3$. So, it can be deduced that the LCMO film depositing on the NdGaO$_3$ exhibits more likely a layer by layer growth mode, whereas LCMO film on LaAlO$_3$ demonstrates an island growth mode. Moon-Ho Jo *et al.*[36] found that LCMO on NdGaO$_3$ exhibits a layer by layer growth mode, whereas Rao *et al.*[37] observed that LCMO on LaAlO$_3$ shows granular-like surface features. These results are consistent with our prediction. Moreover, the BCMO epitaxial films on (110) NdGaO$_3$ and LaAlO$_3$ substrates were also considered. For the BCMO on the NdGaO$_3$ and LaAlO$_3$, the critical thicknesses are 1.72 and 87.90 nm, respectively. For BCMO/NdGaO$_3$, the lattice mismatch is 1.88%, while it is 0.079% for the BCMO/LaAlO$_3$. Therefore, for BCMO on NdGaO$_3$, it exhibits more likely an island growth mode, whereas for BCMO on LaAlO$_3$, it is more likely a layer by layer growth mode. Chaudhuri and Budhani[38] observed that the BCMO on the LaAlO$_3$ has a smooth surface by AFM. This result matches well with our prediction for growth mode for BCMO grown on LaAlO$_3$.

For metal and semiconductor epitaxial films, FvdM, VW, and SK models have been proposed to explain layer by layer, the island and the layer by layer plus the island growth modes. These theoretical models have been experimentally observed, for example, in Au/Ag[39], Au/molybdenite[40], and Ge/Si[18] systems. But for perovskite manganite epitaxial films, no mature growth model has been reported yet. The above three models are based on the interface energy, substrate surface energy, and epilayer surface energy,

but the diffusion of the surface atoms and the lattice mismatch between the substrate and the epitaxial film are not considered. Thus, only one single model cannot explain different systems. Our atom collapse model can account for all the three growth modes. In SK model, it has been reported that Ge film epitaxially grown on a Si substrate can undergo a morphology transition from layer by layer to 3-D island. However, it does not provide the detailed information about this transition process whereas our atom collapse model depicts this transition through the atomic collapse and diffusion. At first, the epitaxial film is strained due to the lattice mismatch between film and substrate. When the thickness of epitaxial film reaches the critical thickness, the atoms begin to collapse and the misfit dislocation starts to form. The atom collapse process transforms the epitaxial manganite film from a flat surface morphology into an island morphology. Our atomic collapse model is more reasonable to explain this growth mode.

IV. Summary

In conclusion, two different growth modes were observed for epitaxial perovskite manganite films, namely, island growth mode and layer by layer growth mode. At the beginning of the deposition of either BCMO or LCMO on STO substrates, the strain caused by the lattice mismatch can be accommodated by elastic deformation. With increase of film thickness, dislocations formed with islands observed for the higher mismatched BCMO and a uniform, layer by layer growth observed for LCMO. The atomic diffusion length for BCMO films was sufficient at the growth temperature to allow the surface strain to be relaxed through formation of islands. Our results could shed light on the growth modes for other perovskite epitaxial films.

References

[1]O. Y. Gorbenko, I. E. Graboy, A. R. Kaul, and H. W. Zandbergen, "HREM and XRD Characterization of Epitaxial Perovskite Manganites," *J. Magn. Magn. Mater.*, **211**, 97–104 (2000).

[2]T. Nakajima, T. Tsuchiya, K. Daoudi, Y. Ueda, and T. Kumagai, "Structural and Physical Property of A-Site Ordered Perovskite Manganite LaBaMn$_2$O$_6$ Thin Film on SrTiO$_3$(001)," *Mater. Sci. Eng., B*, **144**, 104–8 (2007).

[3]A. Malisa and Z. Ivanov, "Colossal Magnetoresistance Effect in Epitaxially Grown La$_{2/3}$Ca$_{1/3}$MnO$_3$ Perovskite-Like Manganite Thin Films," *J. Magn. Magn. Mater.*, **295**, 277–83 (2005).

[4]O. Y. Gorbenko, A. R. Kaul, A. A. Kamenev, O. V. Melnikov, I. E. Graboy, N. A. Babushkina, A. N. Taldenkov, and A. V. Inyuskin, "Epitaxial Variant Structures of the Perovskite Manganites with the High Tunnel Magnetoresistance," *J. Cryst. Growth*, **275**, e2453–8 (2005).

[5]M. J. Casanove, C. Roucau, P. Baulès, J. Majimel, J. C. Ousset, D. Magnoux, and J. Bobo, "Growth and Relaxation Mechanisms in La$_{0.66}$Sr$_{0.33}$MnO$_3$ Manganites Deposited on SrTiO$_3$(001) and MgO(001)," *Appl. Surf. Sci.*, **188** 19–23 (2002).

[6]W. J. Gallagher, S. S. P. Parkin, Y. Lu, X. P. Bian, A. Marley, K. P. Roche, R. A. Altman, S. A. Rishton, C. Jahnes, and T. M. Shaw, "Microstructured Magnetic Tunnel Junctions," *J. Appl. Phys.*, **81**, 3741–6 (1997).

[7]J. Jorzick, S. O. Demokritov, B. Hillebrands, B. Bartenlian, C. Chappert, D. Decanini, F. Rousseaux, and E. Cambril, "Spin-Wave Quantization and Dynamic Coupling in Micron-Size Circular Magnetic Dots," *Appl. Phys. Lett.*, **75**, 3859–61 (1999).

[8]J. F. Feng, K. Zhao, Y. H. Huang, J. G. Zhao, X. F. Han, W. S. Zhan, and H. K. Wong, "Magnetotransport Properties of La$_{0.67}$Ca$_{0.33}$MnO$_3$/ La$_{0.67}$Sr$_{0.33}$MnO$_3$ Bilayers," *Chinese Phys.*, **14**, 1879–81 (2005).

[9]J. Chang, Y. S. Park, J. W. Lee, and S. K. Kim, "Layer-by-Layer Growth and Growth-Mode Transition of SrRuO$_3$ Thin Films on Atomically

Flat Single-Terminated SrTiO$_3$ (111) Surfaces," *J. Cryst. Growth*, **311**, 3771–4 (2008).

[10]H. A. van der Vegt, H. M. van Pinxteren, M. Lohmeier, E. Vlieg, and J. M. C. Thornton, "Surfactant-Induced Layer-by-Layer Growth of Ag on Ag (111)," *Phys. Rev. Lett.*, **68** [22] 3335–8 (1992).

[11]G. H. Lee, M. Yoshimoto, T. Ohnishi, K. Sasaki, and H. Koinuma, "Epitaxial BaTiO$_3$ Thin Films Grown in Unit-Cell Layer-by-Layer Mode by Laser Molecular Beam Epitaxy," *Mater. Sci. Eng., B*, **56**, 213–7 (1998).

[12]X. H. Wei, J. Zhu, and Y. R. Li, "Anisotropic Lattice Strain Relaxation of MgO/SrTiO$_3$(001) in a Textured Island Growth Mode," *Vacuum*, **85**, 999–1003 (2011).

[13]K. Aït-Mansour, D. Dentel, L. Kubler, M. Diani, J. L. Bischoff, and A. Galliano, "Ge Epitaxial Island Growth on a Graphitized C-Rich 4H-SiC (0001) Surface," *J. Cryst. Growth*, **275**, e2275–80 (2005).

[14]D. Liu and W. Liu, "Growth and Characterization of Epitaxial (La$_{2/3}$Sr$_{1/3}$)MnO$_3$ Films by Pulsed Laser Deposition," *Ceram. Int.*, **37**, 3531–4 (2011).

[15]Y. H. Ding, R. S. Cai, Q. T. Du, Y. Q. Wang, Y. Z. Chen, and J. R. Sun, "Microstructure Evolution of Bi$_{0.4}$Ca$_{0.6}$MnO$_3$ Epitaxial Films with Different Thickness," *J. Cryst. Growth*, **317**, 115–8 (2011).

[16]C. W. Snyder, D. Barlett, B. G. Orr, P. K. Bhattacharya, and J. Singh, "The Molecular Beam Epitaxy Growth of InGaAs on GaAs(100) Studied by in situ Scanning Tunneling Microscopy and Reflection High-Energy Electron Diffraction," *J. Vac. Sci. Technol., B*, **9** [4] 2189–93 (1991).

[17]F. K. LeGoues, M. Copel, and R. M. Tromp, "Microstructure and Strain Relief of Ge Films Grown Layer by Layer on Si(001)," *Phys. Rev. B*, **42** [18] 11690, 20pp (1990).

[18]M. Asai, H. Ueba, and C. Tatsuyama, "Heteroepitaxial Growth of Ge Films on the Si(100)-2 × 1 Surface," *J. Appl. Phys.*, **58** [7] 2577–83 (1985).

[19]M. J. Beck, A. Van de Walle, and M. Asta, "Surface Energetics and Structure of the Ge Wetting Layer on Si(100)," *Phys. Rev. B*, **70** [20] 205337, 7pp (2004).

[20]E. Z. Liu and C. Y. Wang, "Energetics of the Growth Mode Transition in InAs/GaAs(001) Small Quantum Dot Formation: A First-Principles Study," *Surf. Sci.*, **600** [10] 2007–10 (2006).

[21]F. C. Frank and J. H. van der Merwe, "One-Dimensional Dislocations. I. Static Theory," *Proc. R. Soc. Lond. A*, **198**, 205–16 (1949).

[22]M. Volmer and A. Weber, "Nucleation in Super-Saturated Products," *Z. Phys. Chem.*, **119**, 277–301 (1926).

[23]I. N. Stranski and Von L. Krastanow, "Abhandlungen der Mathematisch-Naturwissenschaftlichen Klasse," *Akad. Wiss. Lit. Mainz Math. Naturwiss. Kl*, **146**, 797 (1939).

[24]J. H. van der Merwe, "Crystal Interfaces. Part I. Semi-Infinite Crystals," *J. Appl. Phys.*, **34**, 117–22 (1963).

[25]J. W. Matthews, S. Mader, and T. B. Light, "Accommodation of Misfit Across the Interface Between Crystals of Semiconducting Elements or Compounds," *J. Appl. Phys.*, **41** [9] 3800–4 (1970).

[26]J. W. Matthews and A. E. Blakeslee, "Defects in Epitaxial Multilayers. I. Misfit Dislocations," *J. Cryst. Growth*, **27**, 118–25 (1974).

[27]O. I. Lebedev, G. Van Tendeloo, S. Amelinckx, H. L. Ju, and K. M. Krishnan, "High-Resolution Electron Microscopy Study of Strained Epitaxial La$_{0.7}$Sr$_{0.3}$MnO$_3$ Thin Films," *Philos. Mag.*, **80** [3] 673–91 (2000).

[28]H. Sun, J. M. D. Coey, Y. Otani, and D. P. F. Hurley, "Magnetic Properties of a New Series of Rare-Earth Iron Nitrides: R$_2$Fe$_{17}$N$_y$ (y ~ 2.6)," *J. Phys.: Condens. Matter.*, **2**, 6465–70 (1990).

[29]T. H. Jacobs, K. H. J. Buschow, G. F. Zhou, X. Li, and F. R. De Boer, "Magnetic Interactions in R$_2$Fe$_{17-x}$Al$_x$ Compounds (R= Ho, Y)," *J. Magn. Magn. Mater.*, **116** [1–2] 220–30 (1992).

[30]I. W. Boyd, and W. Zhang, "Growth of Perovskite Manganite Oxide Thin Films by PLD," *Appl. Surf. Sci.*, **127–129**, 410–7 (1998).

[31]T. Frey, C. C. Chi, C. C. Tsuei, T. Shaw, and F. Bozso, "Effect of Atomic Oxygen on the Initial Growth Mode in Thin Epitaxial Cuprate Films," *Phys. Rev. B*, **49** [5] 3483–91 (1994).

[32]Y. Z. Chen, J. R. Sun, S. Liang, W. M. Lv, B. G. Shen, and W. B. Wu, "Effect of Anisotropic Strain on the Charge Ordering Transition in Manganite Films," *J. Appl. Phys.*, **103**, 096105, 3pp (2008).

[33]Y. Z. Chen, J. R. Sun, S. Liang, W. M. Lu, and B. G. Shen, "Strain-Controlled Anisotropic Electronic Transport in Bi$_{0.4}$Ca$_{0.6}$MnO$_3$ Films," *J. Appl. Phys.*, **104** [11] 113913–4 (2008).

[34]W. W. Gao, "Electrical, Magnetic and Photoelectronic Properties of Ultrathin Manganite Films and Heterojunctions"; pp.115–6, Ph.D. Thesis, Institute of Physics, Chinese Academy of Sciences, China, 2012.

[35]R. People and J. C. Bean, "Calculation of Critical Layer Thickness Versus Lattice Mismatch for Ge$_x$Si$_{1-x}$/Si Strained-Layer Heterostructures," *Appl. Phys. Lett.*, **47**, 322–4 (1985).

[36]M. H. Jo, N. D. Mathur, N. K. Todd, and M. G. Blamire, "Very Large Magnetoresistance and Coherent Switching in Half-Metallic Manganite Tunnel Junctions," *Phys. Rev. B*, **61** [22] R14905–8 (2000).

[37]R. A. Rao, D. Lavric, T. K. Nath, C. B. Eom, L. Wu, and F. Tsui, "Effects of Film Thickness and Lattice Mismatch on Strain States and Magnetic Properties of La$_{0.8}$Ca$_{0.2}$MnO$_3$ Thin Films," *J. Appl. Phys.*, **85** [8] 4794–6 (1999).

[38]S. Chaudhuri and R. C. Budhani, "Studies of Structural, Magnetic, Electrical, and Photoconducting Properties of Bi$_{1-x}$Ca$_x$MnO$_3$ Epitaxial Thin Films," *Phys. Rev. B*, **74** [5] 054420, 9pp (2006).

[39]J. W. Matthews, "Accommodation of Misfit across the Interface between Single-Crystal Films of Various Face-Centred Cubic Metals," *Philos. Mag.*, **13** [126] 1207–21 (1966).

[40]D. W. Pashley, M. J. Stowell, M. H. Jacobs, and T. J. Law, "The Growth and Structure of Gold and Silver Deposits Formed by Evaporation inside an Electron Microscope," *Philos. Mag.*, **10** [103] 127–58 (1964). □